J. Min. Metall. Sect. B-Metall. 48 (3) B (2012) 419 - 425

Journal of Mining and Metallurgy, Section B: Metallurgy

PHASE DIAGRAM PREDICTION AND PARTICLE CHARACTERISATION OF Sn-Ag NANO ALLOY FOR LOW MELTING POINT LEAD-FREE SOLDERS

J. Sopoušek[a,*], J. Vřešťál[a], A. Zemanova[b], J. Bursik[b]

[a] CEITEC, Masaryk Univerzity, Czech Republic
[b] Institute of Physics of Materials, Academy of Sciences, Czech Republic

(Received 21 January 2012; accepted 06 June 2012)

Abstract

SnAg nanoparticles (SnAg NPs) were prepared by wet synthesis. The chemical composition of the SnAg NPs was messured by inductively coupled plasma - mass spectrometry. The prepared fine powder samples were characterized by electron microscopic technique (SEM) and thermal analysis (DSC). The nanoparticles with different size were obtained. The size dependent melting point depression (MPD) of the SnAg NPs was determined experimentally. The size dependent phase diagram of the SnAg alloy was calculated using CALPHAD method, which has been extended to describe the surface energy of SnAg nanoparticles. The same approach was used for SnAg eutectic MPD calculations. The own experimental and theoretical results were compared with the data of the other authors. The satisfactory agreement was found.

Keywords: *tin, silver, nanoparticle, thermal analysis, DSC, TEM, SEM, CALPHAD.*

1. Introduction

Nanoparticles (NP) may exhibit size-related properties that differ significantly from those observed for a fine micron particle system or for bulk material with the same chemical composition [1-5]. The differences can be found in physical and chemical properties, kinetics, and other features including phase transformations. The melting point depression (MPD) of pure metal nanoparticles, for example pure tin [3] is well documented. Thermodynamic predictions [6] show that also the melting of the alloy nanoparticles (i.e. nanoalloys) is influenced by size. MPD effect is supposed to be caused by high surface-to-volume ratio of nanoparticles.

The melting point depression of metal nanoparticles may give rise to subsequent aggregation and creation of micron particle system, which behave like bulk sample. This can be useful for design of novel technologies. For example, the electrical conductive connection prepared by bulk forming from nanoparticle system at temperatures lower then liquidus for bulk alloy can be interesting alternative for lead-free soldering in the electronics industry.

The Sn-Ag system represents the metal base, which is frequently used for lead-free soldering. This system reveals eutectic point at 219.8ºC / 3.7wt%Ag [7] in bulk form. The size dependent melting of the SnAg nanoparticles (NPs) with composition close to eutectic point was measured by Jiang and co-workers [8]. They made the wet synthesis of the SnAg NPs with nearly SnO2 oxide-free surface covered by organic surfactant. The reported nanoalloy melting point was 194.3ºC for particle diameter 10nm. Pande et al [7] chose another synthetic way and they reached SnAg NPs (size 80nm) with melting point at 228ºC. This example of MPD difference indicates that MPD is influenced by surface covering too [9]. The application of the SnAg NPs prepared via arc discharge process was done by Bao [10]. The lowest observed MPD for (40-50) nm NPs was approx. -9ºC.

The size dependent phase diagrams can be obtained using calculations based on CALPHAD approach [11]. In order to extend the use of CALPHAD approach to small metallic nanoparticles, the Gibbs energy expression has to be extended with an additional parameters describing surface energy [6]. This approach assumes several simplifications. The most fundamental one is that the surface chemistry of nanoparticles is identical with the chemistry of bulk of composition below the surface and that the surface-absorbed substances are not present. Whether we can use this method for predicting the melting point depression of the SnAg NPs is the subject of this work.

2. Experiment

2.1 Sn-Ag nanoparticle preparation

SnAg nanoparticles (SnAg NPs) were prepared by

* *Corresponding author: sopousek@mail.muni.cz*

DOI:10.2298/JMMB120121032S

Dedicated to the memory of Professor Zbigniew Moser

wet synthesis from silver nitrate and stannous ethylhexanoate by reduction with NaBH4 at temperature 0°C, -10°C, and -20°C in methanol under a nitrogen atmosphere [6]. Washing in methanol purified the nanoparticles. The samples of the wet and dry SnAg NPs were isolated by uncompleted and total evaporation of the solvent under vacuum respectively. The all prepared suspensions and dry fine powder of SnAg NPs were manipulated under air.

2.2 Nanoparticle characterisation

The prepared fine powder samples were characterized by electron microscopic technique and thermal analysis.

Each sample of the synthetised SnAg NPs was investigated and analyzed using a TESCAN LYRA3 FEG-SEMxFIB scanning electron microscope (SEM) with EDX analyser. The particles under vacuum inside the microscope revealed tendency to aggregate and form partially necked structure (see SEM micrographs in Figures 1, 2 and 3. The original size of the nanoparticles can be distinguished and measured. The average particle size of 90nm (preparation temperature 0°C), 60nm (-10°C), and 40nm (-20°C) was evaluated with accuracy ±10 nm. The highest aggregation tendency was observed for the smallest particle size synthesised at -20°C (Figure 3.). Our previous studies showed that SnAg NPs observed in transmission electron microscope tended to melt and transform to bigger (micron size) particles directly under the high energy (120 keV) electron beam [12].

It was found by EDX analysis that the majority nano-particle forming components are Ag (2-10wt%) and Sn (98-90wt%). The EDX signal of oxygen was uncertain. The exact contents of silver and tin in the NPs samples were obtained by inductively coupled plasma - mass spectrometry (ICP-MS), which is more accurate than EDX analysis.

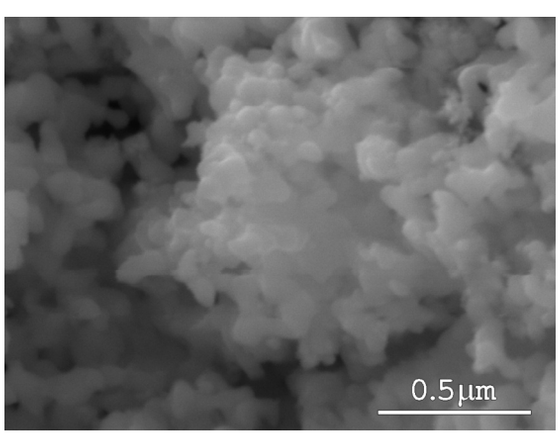

Figure 1. *Structure of the Sn-4.19wt%Ag nano powder synthesized at 0 °C (SEM, average particle size 90 nm).*

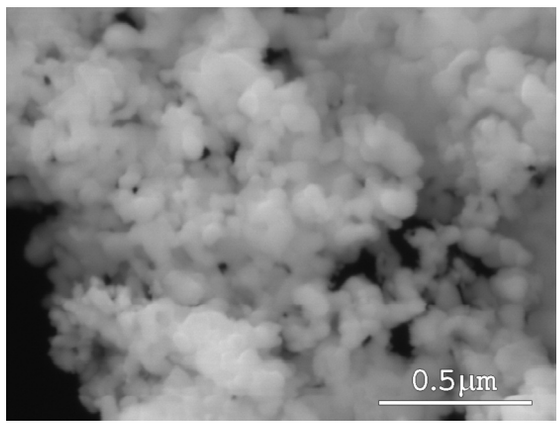

Figure 2. *Structure of the Sn-7.84wt%Ag nanopowder synthesized at -10 °C (SEM, av. particle size 60 nm).*

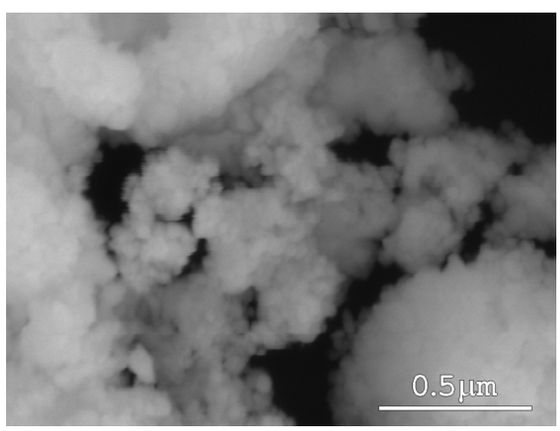

Figure 3. *Structure of the Sn-5.91wt%Ag nanoalloy synthesized at -20 °C (SEM, av. particle size 40 nm and agglomerate ≈1μm (right bottom).*

The each sample of the synthesised SnAg NPs was investigated by thermal analysis in-situ using differential scanning calorimetry (DSC) technique in NETZSCh STA 409 calorimeter (heating/cooling rate 10K/min, Ar 6N atmosphere: 70ml/min) [13]. The DSC method found melting and cooling heat effects at each SnAg NPs sample (see example on Figure 4.). The standard deviation of the MPD measurement is 0.4°C. The first heating cycle was always different from the 2-nd and 3-th heating cycles for each sample. The NP samples after heat treatment turn to micro sized powders i.e. to the objects behaving like bulk materials.

The SnAg NPs prepared at 0ºC reveal (see Figure 4.) the melting point depression –4.3ºC (difference between the nanosized and microsized on-sets of endothermic peaks at 1st and 2nd heating). The first endothermic peak is followed by exothermal effect in temperature range approx. 230-270ºC. The consequent heating sequences do not reveal this

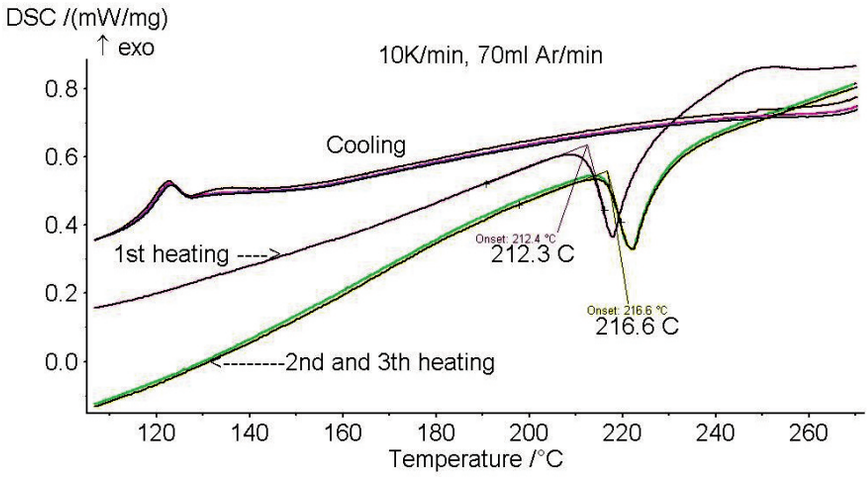

Figure 4. *DSC heating and cooling curves of Sn-4.19 wt%Ag nanoalloy (90nm, synthesized at 0 °C).*

exothermal effect and all cooling curves reveal peaks of solidification at temperature range approx. 150-110ºC. The occurred micro sized melting point was put to be equal to bulk eutectic melting temperature 219.8ºC [7]. The experimental differences between nanosized and microsized nanoparticle melting points are given in Table 1.

The SnAg NPs prepared at -10ºC behave similarly to those prepared at 0ºC moreover they reveal higher melting point depression -6.3ºC. The SnAg NPs prepared at -20ºC reveal nanosized endothermic peak at 1st heating cycle (MPD: -11.2ºC), which is followed by second endothermic peak (see detail in Figure 5.).

Table 1. *Experimental characterisation of the SnAg NPs.*

Synthesis temperature / ºC	Chemical composition (ICP-MS)) / at%	Nanoparticle diameter (microstructure) / nm	Melting point depression / ºC (DSC curve)	Predicted (CALPHAD) eutectic temperature depression / ºC
0	4.19	90nm (unimodal)	-4.3 (sharp peak)	-4.5
-10	7.84	60nm (unimodal)	-6.3 (sharp peak)	-7.7
-20	5.91	40nm and ≈1μm (bimodal)	-11.2 (double peak)	-12.5

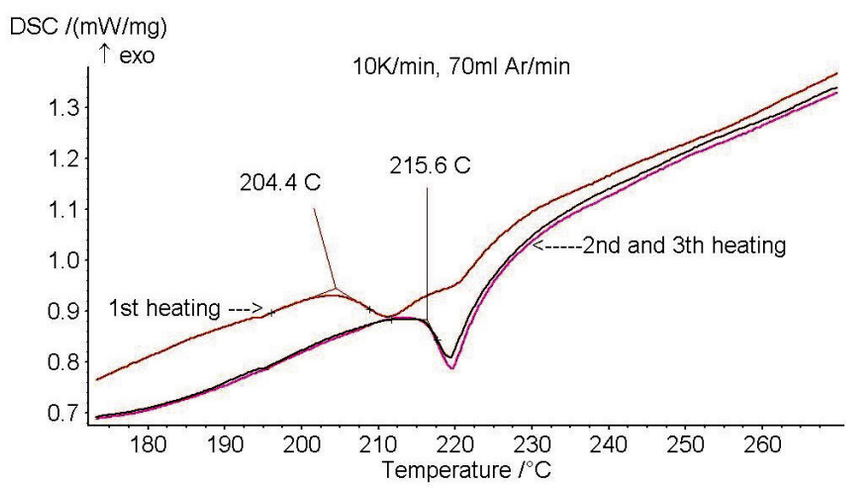

Figure 5. *DSC heating and cooling curves of Sn-5.91 wt%Ag nanoalloy (40nm and 1μm, synthesized at -20°C).*

3. Thermodynamic calculation of nano phase diagram

Phase diagrams of nanoalloys differ from the phase diagrams of bulk systems by including the third variable – size of nanoparticles. The function for binary system (x is composition and r radius of particle) is to be determined. Nanoparticles, particles with dimension 5 – 100 nm, have increasing surface to volume ratio with decreasing dimension and bring therefore substantial contribution of surface energy to Gibbs energy for thermodynamic considerations. Chemical potential of pure substances and the excess Gibbs energy need, therefore, to be described as a function of temperature, composition and particle size.

The method, presented by Park and Lee [6] for Ag-Au system was used in this work for calculation of phase diagram of Ag-Sn system. CALPHAD method used in [6] is based on the minimization of the molar Gibbs energy of the entire system G^{tot}, which is defined as

$$G^{Total} = \sum_f \left(G^{Bulk,f} + G^{Surface,f} \right) \quad (1)$$

where $G^{Bulk,f}$ and $G^{Surface,f}$ are Gibbs energies of the bulk and of the surface of the A-B binary phase f, respectively. The Gibbs energy of the bulk of the phase f $G^{Bulk,f}$ is expressed in a standard way:

$$G^{Bulk,f} = x_A {}^0G_A + x_B {}^0G_B + RT\left(x_A \ln(x_A) + x_B \ln(x_B)\right) + G^{E,Bulk,f} \quad (2)$$

where x_A, x_B are molar fractions of components A and B in phase f, respectively. ${}^0G_A$, ${}^0G_B$ are the standard Gibbs energies of A and B in f phase structure, R is the gas constant and T the temperature. $G^{Bulk,f}$ is the excess Gibbs energy of the bulk of phase f, expressed usually by Redlich-Kister polynomial

$$G^E = x_A x_B \sum_i L^i(T) \cdot (x_B - x_A)^i \qquad (i = 0, 1, 2, \ldots) \quad (3)$$

$$L^i = a_i + b_i T + c_i T \ln T. \quad (4)$$

The Gibbs energy of the surface of the phase f, $G^{Surface,f}$, is expressed for isotropic spherical particles by

$$G^{Surface,f} = 2 C_f \sigma_f V_f / r \quad (5)$$

where σ_f is the surface tension, V_f is the molar volume, C_f is a correction factor considering the effects from the shape, the surface strain due to non-uniformity and the uncertainty of the surface tension measurements [6] of the phase f. The value of C_f for liquid and for fcc solid phase were estimated to be 1.00 and 1.05, respectively [6].

The exploitation of eq.(5) for calculation of surface energy correction for pure elements is straightforward. Excess Gibbs energy for bulk alloys is used for nanoallys unchanged in the first approximation used in this work. Correction factors, C_f surface tensions, σ_f, and molar volumes, V_f, for all solid phases (FCC, HCP, BCT) are approximated by the same value, for σ_f and V_f given in the Table 2. For Ag3Sn compound, the proportional correction of surface energy was added ($0.75*G_{Ag}^{surf,FCC} + 0.25*G_{Sn}^{surf,BCT}$) to the bulk value:

$$G^{Ag3Sn,Ag:Ag}(J/mol) = GHSERAG + 5000 + 3.94E - 05 * RR - 1.10609E - 08 * RR * T$$

$$G^{Ag3Sn,Ag:Sn}(J/mol) = -11085.3 + -110.01471 * T - 23.18 * T * LN(T) - -0.00359 * T**2 + 4389.5 * T**(-1) + +3.58E - 05 * RR - 6.49E - 09 * RR * T$$

where (RR = 1/r) means reciprocal radius.

We have used Gibbs energies of pure elements, displayed in the [19], for CALPHAD type calculation of phase diagram of Ag-Sn system. As shown above, introduction of correction $G^{surface,f} = 2 C_f \sigma_f V_f / r$ (product of $\sigma_f(T).V_f(T)$) for every element to the Gibbs energy polynomial of pure components in individual phases was performed. The same correction for all solid structures (FCC, HCP and BCT) of both pure elements (Ag and Sn) and no (excess) surface tension corrections for nano-alloys in this step was done. By this way, the Gibbs energy function, depending on the size of nanoalloy particles (via reciprocal radius) in respective phases [2], for phase diagram of nanoalloys calculation, were used.

Phase diagram, calculated on this basis is shown in the Figure 6. for bulk alloys and in the Figure 7. for the nanoalloys with d = 40 nm.

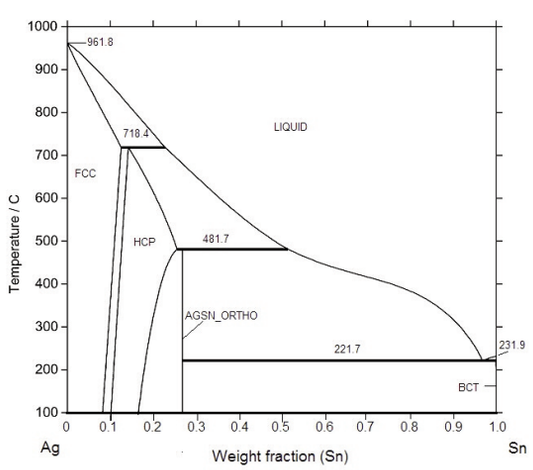

Figure 6. *Calculated phase diagram of Ag-Sn bulk.*

Table 2. *Physical properties of Ag and Sn elements*

Surface tension:		
$\sigma_{Ag}^{L}(N/m) = 1.207 - 2.28\times10^{-4}T$	(T in K)	[14]
$\sigma_{Ag}^{S}(N/m) = 1.675 - 0.47\times10^{-3}T$		[15]
$\sigma_{Sn}^{L}(N/m) = 0.5828 - 0.8343\times10^{-4}T$		[16]
$\sigma_{Sn}^{S}(N/m) = 0.729 - 1.4\times10^{-4}T$		[16]
Molar volume:		
$V_{Ag}^{L}(m^3/mol) = 1.0198\times10^{-5} + 1.1368\times10^{-9}T$		[17]
$V_{Ag}^{S}(m^3/mol) = 1.12066\times10^{-5}$	(at room temperature)	[17]
$V_{Sn}^{L}(m^3/mol) = 1.70\times10^{-5}$		[18]
$V_{Sn}^{S}(m^3/mol) = 1.62\times10^{-5}$	(at room temperature)	[18]

Excess molar Gibbs energy (bulk alloy): - source: database [7]	
$G^{E,L,AgSn}$ (J/mol) – eq. (3):	L^0 = -3177.49-10.1612*T+.380505*T*LN(T)
	L^1 =16782.2+2.06521*T+.437477*T*LN(T)
	L^2 =3190.34 +107.094*T+13.9548*T*LN(T)
$G^{E,BCT}$(J/mol) – eq. (3):	L^0 = 18358.8
$G^{E,FCC}$(J/mol) – eq. (3):	L^0 = 745.45 + 11.498027*T
	L^1 =-36541.5
$G^{E,HCP}$(J/mol) – eq. (3):	L^0 = 1046.1+10.23693*T
	L^1 =-40505.5
$G^{E,Ag3Sn}$ (J/mol) – eq. (3):	L^0 = 0

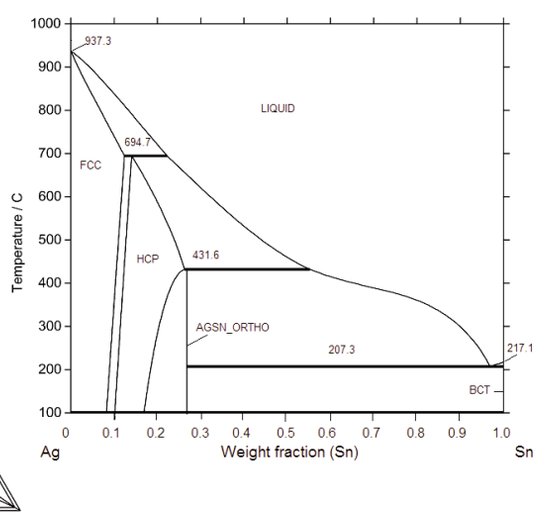

Figure 7. *Predicted phase diagram of SnAg NPs (40 nm).*

4. Discussion

The suspensions with different average sizes of the SnAg NPs were prepared by wet synthesis. It was confirmed that the decrease in temperature of synthesis [8] leads to the formation of smaller nanoparticles. The resulting nano product can be kept as a suspension or as a dry powder of SnAg NPs.

The experiment shows that SnAg nanoparticles have a strong tendency to aggregate. This effect occurs within the time of preparation and storage. The aggregates are formed after evaporation of the organic liquid phase and after surfactant layer disturbances that take place in high vacuum inside electron microscope (see Figure 1., Figure 2., and Figure 3.). This behavior can be explained by assumption that the surface of the nanoparticles becomes active metallic surface, which is free of oxides and other substances.

Extra heating of the SnAg NPs aggregates by energy absorption of the high energy electron beam in TEM can get rise to bigger SnAg particles.

The SnAg NPs compositions (see Table 1) determined by ICP-MS show that the samples have the chemical compositions outside eutectic (Sn-3.8 wt% Ag). However, the DSC signal of each SnAg NP sample appears like the eutectic signal of bulk at temperature, which is referred here as MPD (see Table 1.). Any additional effects on the DSC signal during melting SnAg NPs cannot be attributed to the sample signal below or above the eutectic composition. The second endothermic peak at 1st heating curve (see on-set 216.5°C on Figure 5.) is the DSC signal of SnAg microparticle melting. On the other hand, an exothermic peak (region (230-250)°C on Figure 4.) may be caused by SnAg nanoparticle aggregation or by oxidation of organic surfactant by O2 impurities inside inert gas.

Experimentally found the MPD values of the samples are shown in Table 1. The respective experimental dependences of T_m(Sn-nano) and T_e(SnAg-nano) on the size of nanoparticles are plotted in Figure 8. These results are compared there with the results of other authors and with the theoretical results obtained by means of CALPHAD approach.

If we assume that other authors have measured in the case of the SnAg nanoparticles their nanoparticle size dependent eutectic temperature, we can observe, on the Figure 8. good agreement between the theoretical curves T_m(Sn-nano) and T_e(SnAg-nano) from work [8] and [10] and the discrepancy with the work [9].

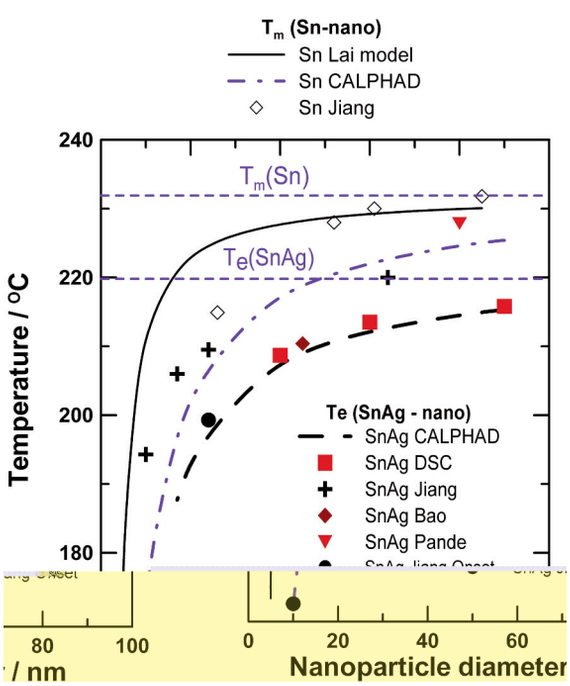

Figure 8. *Experimental and theoretical dependences of pure Sn nanoparticle melting T_m(Sn-nano) and SnAg nanoparticle eutectic temperature T_e(SnAg-nano) on the particle size.*

The CALPHAD method provides (if the surface energy omitted) Sn bulk melting point T_m (Sn) = 231.9°C and SnAg eutectic temperature T_e(SnAg = 219.8 °C (compare Figure 8.). It is obvious that these transformation temperatures decrease with the nanoparticle size (i.e. MPD grows) if we introduce surface term. The predicted size dependences of T_m(Sn-nano) and T_e(SnAg-nano) are in satisfactory agreement with the experiments. Moreover, the agreement turn to excellent when the on-sets from original figures in work [8] are plotted. This consistency suggests that the transformation temperature of nanoparticle depends mainly on the bulk thermodynamic properties and surface energy contribution. Other influences are less important.

5. Conclusions

The SnAg nanoparticles with different size were prepared experimentally by synthetic route under temperature control. The exact compositions SnAg NPs were determined by ICP-MS. The chemical compositions of the prepared samples were different from the SnAg eutectic composition. The SnAg NPs were characterised by means of scanning electron microscopy. The average size was evaluated and the aggregation effect occurred.

The size dependent phase diagram of the SnAg alloy was calculated using CALPHAD method, which has been extended to describe the surface energy of SnAg nanoparticles. This theoretical approach allowed obtaining the size dependent SnAg phase diagram boundaries involving the liquid phase. The eutectic temperature was of the most importance.

Although the sample composition of the nanoparticles was not eutectic, the shape of the DSC signal typical for bulk alloys with the under/above eutectic composition was never observed. The signal reveals like to DSC signal of pure nanometals [4]. This fact may indicate that the coexistence of liquid and solid phases inside individual SnAg alloy nanoparticle either does not follow strictly the rules for bulk phase equilibrium system [20] or the thermodynamic equilibrium is influenced by envelope consisting from surfactant. This fact should be taken into account and investigation of the impact of it on application of nanoparticles SnAg as alternatives to lead-free soldering is desirable.

The DSC method was used to determine the thermal effects accompanying the heating of the SnAg nanoparticles. The eutectic melting point depression of the SnAg nanoparticles was observed. The experimentally obtained results were compared with

the theoretical ones, which were predicted by CALPHAD approach complemented with surface term. The findings were also compared with the experimental results of other authors. The experimental and calculated eutectic temperatures were found to be in satisfactory agreement.

Acknowledgement

Financial support of the Czech Science Foundation (grant No. 106/09/0700) and of Ministry of Education, Youth and Sports of the Czech Republic (MPO903/LD11046, CEITEC MU CZ.1.05/1.1.00/02.0068) is gratefully acknowledged.

References

1. P.Z. Pawlow, Phys. Chem., 1 (1909) 65.
2. J. Park, J. Lee, Calphad, 32 (2008) 135.
3. H. Jiang, K. Moon, H. Dong, F. Hua, and C.P. Wong, Chemical Physics Letters, 429 (2006), 492.
4. J. Sopousek, J. Bursik, J. Zalesak and Z. Pesina, J. Min. Metall. Sect. B-Metall. 48 (1) B (2012) 63-71.
5. R. Ahmadi and H. R. Madaah Hosseini, J. Min. Metall. Sect. B-Metall. 48 (1) B (2012) 81-88
6. J. Lee, T. Tanaka, J. G. Lee, H. Mohri, Calphad, 31 (2007) 105.
7. A.T. Dinsdale, A. Watson, A. Kroupa, J. Vrestal, J.Vizdal, A. Zemanova, Solders, thermodynamic database for lead free solder systems. UK: National Physical Laboratory, 2008.
8. H. Jiang, K. Moon, F. Hua, C.P. Wong, Chem. Mater. 19 (2001), 4482.
9. S. Pande, A.K. Sarkan, M. Basu, S. Jana, A.K. Sinha, S. Sarkar, M. Pradhan, S. Saha, A. Pal, Langmuir, 24 (2008), 8991.
10. T.T. Bao, Y. Kim, J. Lee, J.G. Lee, Metallurgical Transactions, 51 (2010) 2145.
11. N. Saunders, A. P. Miodovnik, 'CALPHAD, Pergamon Materials Series, Vol.1, Elsevier Science, Amsterdam (1998).
12. J. Buršík, D. Škoda, V. Vykoukal, J. Sopoušek, In: NANOCON 2011, Proceedings on CD, Brno, Czech Republic, 2011.
13. Z. Pešina, J. Sopoušek, Application of the simultaneous DSC/DTA/QMS thermal analyse to alloy and nanopowder characterization, In B. Katalinic. Annals of DAAAM for 2011 & Proceedings. Vienna: DAAAM International Vienna, 2011. pp. 1657-1658. ISSN 1726-9679.
14. J. Lee, W. Shimoda, T. Tanaka, Mater. Trans., 45 (2004) 2864.
15. J. Lee, M. Nakamoto, T. Tanaka, J. Mater. Sci., 40 (2005) 2167.
16. R.C. West, Handbook of Chemistry and Physics, 52, 1971/72, Chem. Rubber Co., Ohio 1972.
17. T.Iida, R.I.L. Guthrie, The Physical Properties of Liquid Metals, Oxford Science Publ., 1993.
18. R. Picha, J. Vrestal, A. Kroupa, Calphad, 28 (2004) 141.
19. A.T. Dinsdale, Calphad, 15 (1991) 317.
20. W.A. Jesser, R.Z. Shneck, W.W. Gile, Phys. Rev. B, 69 (2004), 144121.